# MANGANESE PARTITIONING DURING HYDROUS MELTING OF PERIDOTITE

By

J. Brian Balta

Paul D. Asimow

Jed L. Mosenfelder

**ABSTRACT**

Manganese contents and the iron/manganese ratio of igneous rocks have been used as a method of probing the heterogeneity in the Earth's mantle during melting of peridotite and pyroxenite lithologies. Most previous work has assumed that changes in these parameters require changes in either source lithology or composition based on experiments that suggest manganese is slightly incompatible during melting and that the iron/manganese ratio is fixed by the presence of olivine. However, the presence of volatiles in the mantle drives melting at lower temperatures and with different compositions than is seen in volatile-free systems, and thus the partitioning behavior of Fe and Mn may in fact vary. We have produced silicate liquids in equilibrium with a peridotite assemblage under hydrous conditions at 3 GPa pressure which show that manganese can also be unexpectedly compatible in garnet at 1375 °C and Mn partitioning between solids and liquids can be strongly affected by temperature and liquid composition. The compatibility of Mn in garnet provides a mechanism for large variations of Mn contents and the Fe/Mn ratio in silicate melts solely involving melting of mantle peridotite with fairly small compositional changes. Correlations between Mn variations and other indices indicative of melting in the presence of garnet may provide a means of more completely understanding the role of garnet at high pressures in peridotite melting.

## 1. INTRODUCTION

Interpretation of the sources of silicate melting based on the chemical composition of the final products of the melting process is a key goal of modern geochemistry. A common method of interpreting heterogeneity in the mantle source is to identify changes in chemical tracers that are typically associated with variations in lithology or mineral content. A caveat to this technique, however, is that proper application requires a full understanding of all the possible changes taking place within the melting system, as trace element behavior can be strongly influenced by the presence of single minerals or small changes in partitioning under certain conditions. Thus, constraining the inverse problem of identifying mantle source components from observed igneous rocks requires a detailed experimental understanding of the possible changes taking place in the melting region.

Manganese (Mn) contents of igneous rocks and minerals have recently assumed a key role in several geochemical debates. Modern electron microprobes and laser-ablation ICP-MS systems have allowed for analyses of Mn in igneous rocks and minerals at a level of precision that was not previously available. Thus, small changes in Mn contents that were previously difficult to measure have recently drawn attention as petrogenetic indicators.

Sobolev et al. (2007) noted that Mn contents and the Fe/Mn ratio of olivine grains from a variety of melting environments correlated with geochemical indices that suggest the absence of olivine in the melting source, such as nickel contents in magnesium-rich olivine phenocrysts. For example, high Ni-olivines also tended to be high-Fe/Mn olivines. They interpreted the changes in Mn contents and Fe/Mn ratios as related to the removal of olivine from the melting source region through the production of hybridized

pyroxenites, which changes the relative bulk partition coefficients for the oxides in question and produces liquids with elevated Fe/Mn ratios. Gurenko et al. (2009) expanded upon this concept to present an equation that allowed for the calculation of the fraction of pyroxenite in the mantle source based on Ni, Fe, and Mn contents, and a model for the partitioning of each of those elements.

Other possible mechanisms involving variation in Mn contents have been proposed. Qin and Humayun (2008) performed high-precision laser ablation ICP-MS measurements of Fe/Mn ratios in glasses and found variations in the Fe/Mn ratio between different hotspot systems that were larger than the within-volcano variations assigned to the influence of source-pyroxenite by Sobolev et al. (2007). Qin and Humayun (2008) concluded that the variation in Fe/Mn ratio could only be produced by independently varying the Fe and Mn contents in the source rock, and as they could give no obvious globally available reservoir for Mn, they suspected interaction with an iron-rich source, such as the outer core.

These conclusions regarding source components can only be made with experimental knowledge of the partitioning of Fe and Mn between solid phases and liquids during melting under all potentially accessible conditions, including volatile-driven melting. While there is some MnO partitioning data at lower pressures, the best data for the higher pressures that may be reached in ocean island basalt (OIB) and some mid-ocean ridge basalt (MORB) systems comes from Walter (1998), who investigated melting at high temperatures from 3 to 7 GPa. Other studies, including Pertermann and Hirschmann (2003), have provided partitioning measurements during pyroxenite melting. These data have been widely applied, but they do not represent a complete sampling of the behavior

of peridotite melting, as they were all performed under volatile-free conditions and at higher temperatures than may be available through much of the present-day mantle. In addition, some phases that should be stable throughout portions of the melting region only appear in certain experiments, and thus it may be difficult to fully characterize their effect on chemistry throughout the melting column.

We have produced a series of melting experiments on hydrous peridotite from 3 GPa, that will allow us to better constrain the melting relations under different pressure (*P*) and temperature (*T*) conditions than those examined by Walter (1998). From these experiments, we present high-precision analyses of MnO partitioning between peridotite and basaltic liquids that suggest that volatile-driven melting of garnet-bearing lithologies is an additional mechanism for creating variability in MnO contents and Fe/Mn ratio in basalts worldwide.

## 2. ANALYTICAL TECHNIQUES

Major element compositions and volatile compositions for solids and liquids from experiments at 1375 °C are given in Chapter 2. Additional analyses were undertaken for this study to better constrain the MnO content of the phases. All analyses were conducted using the Caltech JEOL JXA-8200 electron microprobe in wavelength dispersive mode. As high-precision analyses of low-concentration elements were necessary in this study, we used several different sets of analytical conditions. All analyses were performed with an accelerating voltage of 15kV. Initial survey measurements of the solid phases were conducted with count times of 20 s on-peak and 10 s off-peak, with a spot size of <1 μm and beam current of 30 nA. Initial survey measurements of the liquids were conducted with identical count times, a current of 10 nA, and a spot size of 15 μm.

Higher-precision measurements of MnO contents were conducted using higher currents and longer count times. For the solid phases, the current was increased to 100 nA, and the count time for MnO was increased to 100 s on-peak and 50 s off-peak. For the liquids, the same long count times were used for MnO, but the current could not be increased as much without excessive damage to the sample. By shortening the counting time for sodium and potassium by a factor of two, we were able to maintain reasonable analyses of the major elements up to a current of 30 nA while simultaneously producing higher-precision analyses of MnO. Analyses using higher currents up to 60 nA were also done, but these produced significant loss of sodium. No difference in the accuracy or precision of MnO analyses were found between the analyses at 30 nA and 60 nA, and thus the data for MnO under both conditions was used, but only the data at lower currents was used for other oxides. The increased counting time and current typically produced a decrease in the variation in MnO by a factor of two compared to the survey analyses. The highest 1σ absolute deviation observed within the measurements of any single experiment was 0.008%, and values below 0.005% were typical.

## 3. RESULTS

### 3.1. 1375 °C Experiments

Each experiment produced a volatile-rich basaltic liquid in contact with a garnet peridotite. Some crystallization of olivine, clinopyroxene (cpx), and garnet always occurred in the outer capsule, giving each experimental charge up to two analyzable sets of liquid-crystal pairs for each solid phase. Differences in the liquid composition between the outer and inner capsules were small (less than 10% for all elements) except for volatile elements, although the inner capsules often suffered more alteration on quench.

Substantial modification of the runs did occur upon quench. Interstitial liquid often rapidly crystallized on the edges of preexisting grains, and pargasitic amphibole often crystallized against the capsule walls. However, in each reported experiment, large pools of unaltered silicate glass and piles of solid crystals were found and analyzed. Compositional results for the elements in question for these experiments are given in Table 1.

A number of techniques suggest that these pairs represent equilibrium assemblages from which representative partition coefficients could be calculated. First, measurements of the olivine/liquid $K_D$ parameter give similar values from experiment to experiment. These values are also close to those seen in other hydrous experiments (e.g, Gaetani and Grove, 1998) and those calculated using calibrations for the variation of this parameter (e.g., Toplis, 2005). The olivines were slightly more iron-rich than those reported by Walter (1998). A few experiments showed $K_D$ values that differed from the average, possibly suggesting disequilibrium or alteration on quench did occur in those experiments. However, the measured partition coefficients for FeO and MnO did not substantially diverge from the values measured in the other experiments.

Second, the solid grains produced during these runs were typically in the range of 5 to 30 microns. Olivine grains were generally the largest. Limited evidence of zoning was found in the solids, including in clinopyroxene, in which Fe/Mg exchange is expected to be the slowest out of the available solids (e.g., Brady and McCallister, 1983; Cherniak, 2001). For garnets in the shortest run, the Mg# (= 100 * molar MgO/(MgO + FeO*)) was found to be 80.9 ± 1.0, a level of heterogeneity on the order of the errors on the probe analyses for those elements and similar to that found in experiments up to three

times as long. Clinopyroxenes and olivines typically showed a similar level of heterogeneity. Zoning that could indicate disequilibrium was minimal and did not increase or decrease with increasing run time, which could happen if there was substantial disequilibrium or loss of components from the capsules at a rate faster than the rate of equilibration between the solids and liquids. Both the lack of zoning and the lack of any correlation between run times and variation in electron probe analyses argue that the experiments represent equilibrated assemblages.

The partition coefficients $D_{MnO}$ (= concentration of species in a solid phase/concentration in liquid) are plotted against $D_{FeO}$ for each of the solid phases present in Figures 1-3. The data of Walter (1998) from a variety of pressures collapse to well-defined lines when the partition coefficients are plotted against *T*, but show at most weak correlations with *P* even when considered at a constant *T*. However, the olivine/melt partition coefficients of these two oxides are strongly correlated with each other and with experimental *T* in both our experiments and in those of Walter (1998), suggesting that this plot is a natural way to visualize our results. In the range from 3 to 7 GPa, therefore, it appears *P* has a much smaller impact on these partition coefficients than *T*, and as such we will not explicitly consider changes in partition coefficients with *P*. When plotted against *T* or against each other, our olivine/melt partition coefficients lie along the same linear trend defined by the other olivine/melt partition coefficients. Both $D_{MnO}^{olivine/melt}$ and $D_{FeO}^{olivine/melt}$ increase with decreasing *T* such that our data for hydrous experiments, although they lie on the same line as those of Walter (1998), occupy a distinct field in Figure 1. The clinopyroxene/melt partition coefficients for both MnO and FeO plot in a small field overlapping the values from Walter (1998); the range of values measured

during peridotite melting is very small and it is difficult to recognize any systematic relationship among $D_{MnO}^{cpx/melt}$, $D_{FeO}^{cpx/melt}$, and *T* (Figure 2).

Surprisingly, in all our experiments, MnO was observed to be compatible in garnet, with an average solid/liquid partition coefficient for garnet measured to be ~1.5. The partitioning of MnO was measured in every experiment to be $D_{MnO}^{garnet/melt} > D_{MnO}^{olivine/melt} > D_{MnO}^{cpx/melt}$, with garnet being the only phase showing a MnO partition coefficient greater than unity. This is surprising, insofar as MnO is slightly incompatible in garnet in all the experiments of Walter (1998). Furthermore, the new data clearly lie well above the extrapolation of the correlation line between $D_{MnO}^{garnet/melt}$ and *T* among the Walter (1998) data (Figure 3).

**3.2. 1250 °C Experiments**

These experiments produced a dacitic liquid with ~6% $H_2O$ in the inner capsules (based on the calibration of Ohlhorst et al., 2001) sitting in contact with solid garnet, orthopyroxene, clinopyroxene, and olivine. The outer capsules were typically completely liquid. Quench features were limited to thin layers occasionally occurring on the outside of solid grains. Unlike the basaltic liquids, the higher silica liquids did not wet all grain boundaries, which may have reduced the ability of the solids to fully equilibrate with the liquids. Because of a combination of this effect and the lower *T*, these experiments did not attain chemical equilibrium during the run duration and may have required substantially longer times (run durations were limited by the diffusion of carbon through the capsules, which became measurable after 24 hours). This is most easily seen in the preservation of Fe-Mg zonation in garnets, which averaged Mg# of 86.7 ± 2.0, a larger range than seen in the higher-*T* experiments.

MnO contents also did not attain equilibrium between the solid phases and the liquids during the duration of the experiments, and garnets in particular showed a very large range in composition across a full order of magnitude. The garnets that were loaded into the experiment initially had 0.19% MnO in them. In the final results, a range in MnO contents in garnet was found from values similar to the initial content (0.20%) up to 2.5% MnO, with an average MnO content of 0.93%. The zoning prevents the calculation of an equilibrium partition coefficient at this *T*. However, the results are still instructive. At this *T*, the compatibility of MnO in garnet appears to be further enhanced. Compared to the experiments at 1375 °C, the liquid formed at 1250 °C is depleted in MnO by a factor of four. This large depletion and the large range in MnO contents suggest that the garnets that came into contact with the liquid incorporated virtually all of the available MnO into their structures, leaving little MnO for the other garnets that did not initially contact the liquid. The low cation diffusivity at this *T* preserves the variable MnO contents for the duration of the run. Although the calculation of an exact partition coefficient is impossible, our measurements show partition coefficients for garnet between 10 and 50 at these conditions. These values are similar to the measured values for $D_{MnO}^{garnet/melt}$ from Patino-Douce (1995) from melting experiments involving tonalitic sources at temperatures from 1000 °C to 1150 °C. Measuring higher values of $D_{MnO}$ using standard electron probes could be difficult because the MnO content of the liquid has decreased to nearly the analytical precision.

$D_{MnO}^{cpx/melt}$ is similar to that measured at 1375 °C and cannot be distinguished given the low concentrations in the low-*T* runs. The olivine appears to have lower MnO contents than those recorded at 1375 °C by a factor of about 1.5, suggesting that the

garnet may have taken up MnO from the olivines as well. $D_{MnO}^{olivine/melt}$ however increased compared to lower *T* runs due to the drop in MnO contents in the liquid. Partition coefficients in the range measured in this experiment also diverge significantly from the linear trend of partition coefficients versus *T* defined by the experiments of Walter (1998), again suggesting that $D_{MnO}$ for all phases likely increases substantially in higher-silica liquids generated at lower *T*.

## 4. DISCUSSION

The experiments of Walter (1998) have formed the basis of a number of analyses of peridotite melting from *P* of 3GPa and higher. There are many advantages to that data set due to the quality of experiments and coverage of *P* and *T* conditions reached by few other experiments. However, the volatile-free nature of those experiments limited them to higher-*T* conditions than are expected in the upper mantle away from all but the highest *T* locations such as, potentially, Hawaii or Iceland (Putirka, 2005). Our experiments show that rich behavior in manganese partitioning can occur during lower-*T* hydrous melting.

### 4.1 MnO partitioning in olivine

Wang and Gaetani (2008) performed experiments at lower temperatures (1200-1350 °C), equilibrating melts of variable composition with large olivine grains to measure partitioning during crystallization. The authors argue that during crystallization of olivine, the main control on the olivine/liquid partition coefficient for MnO is the degree of polymerization of the silicate liquid, parameterized by the ratio of non-bridging oxygens to tetrahedrally-coordinated cations, NBO/T. In their analysis, $D_{MnO}^{olivine/melt}$ is expected to decrease as the NBO/T parameter increases or as the temperature increases.

Hydrous melts present an interesting puzzle for this analysis. Typically, melts from higher *T* are expected to show higher NBO/T, as shown by the experiments of Walter (1998), where the highest-*T* experiments showed the highest fraction of network modifying cations, such as MgO, FeO, and CaO. In those experiments, MnO is most compatible in olivine at the lowest *T* and thus also at the lowest values of NBO/T, consistent with the relation suggested by Wang and Gaetani (2008). Hydrous melts are produced at lower *T*, and thus can have lower concentrations of the network-modifying cations, but water itself is a very strong network modifier due to its ability to react with bridging oxygen to give separate $OH^-$ species as seen in infrared spectra (e.g., Mysen et al., 1980; Dixon and Stolper, 1995). Furthermore, the low mass of hydrogen compared with other typical major elements suggests that per unit mass, water should be particularly effective at increasing NBO/T. Thus, while the lower temperatures are expected to decrease NBO/T, the increased water contents would act to counteract that effect. The precise effect of water on NBO/T is difficult to compute because water is also present in silicate melts as molecular $H_2O$ (which does not consume bridging oxygens) and the details of this speciation are not fully known as functions of *P*, *T*, water content, and major-element composition of the melt.

In our experiments, MnO is measurably more compatible in olivine than in any of the experiments by Walter (1998), but the measured partition coefficients sit on linear trends against *T*, $D_{FeO}^{olivine/melt}$, or $D_{MgO}^{olivine/melt}$ (Figure 1). If the hydrogen is acting to significantly increase NBO/T, then this behavior is surprising and difficult to predict based solely on consideration of NBO/T. In this case, although melt composition may

have some separate effect, it appears that the decreased *T* is a more straightforward and reliable variable for the prediction of $D_{MnO}^{olivine/melt}$.

While we currently know of no adequate calibration for the variation of NBO/T with the addition of water in the compositional range reflected by our basalts, we propose that taking advantage of empirical calibrations for the interaction of olivine and melt may allow for an adequate predictive model of $D_{MnO}^{olivine/melt}$. Toplis (2005) produced an empirical calibration for the variation in the olivine/liquid Fe/Mg $K_D$ that includes the effects of *T*, *P*, and a number of liquid compositional variables, including the water content. Wang and Gaetani (2008)'s model for MnO partitioning included an expression where the effects of NBO/T and the other variables is eliminated algebraically such that $D_{MnO}^{olivine/melt}$ is solely a function of the partition coefficient $D_{MgO}^{olivine/melt}$. Combining our data, the data of Walter (1998), and the basaltic data from Wang and Gaetani (2008), we can calculate a fit that allows for a predictive calculation of the partition coefficient under the full range of conditions considered here, and potentially across the range of conditions for which the Toplis (2005) calibration is accurate. From a least-squares regression to the full data set, the best fit is:

$$Ln\,(DMnO) = 0.82 \times Ln\,(DMgO) - 1.20, \quad (1)$$

which yields fit parameters close to those calculated by Wang and Gaetani (2008) over a more narrow range of *T* and *P*. This calculation shows that MnO is in general more compatible in olivine during melting at lower *T* and suggests that variation in the NBO/T parameter due to hydrous melting produces a limited impact in these basaltic liquids, as shown in our experiments.

**4.2 MnO partitioning in pyroxene**

Pertermann and Hirschmann (2003) performed partial melting experiments on cpx-rich lithologies which provide an additional data set from 3 GPa pressure and temperatures from 1275 °C to 1500 °C that can be compared with our data and that of Walter (1998). Although the trend is not linear, there is a fairly smooth trend with *T* through both the experiments of Pertermann and Hirschmann and the experiments of Walter (1998). While the data from Walter (1998) on their own only define a weak trend against *T*, the experiments of Pertermann and Hirschmann show significant increases in the partition coefficients for FeO, MnO, and MgO with decreasing *T*. Our experiments show partition coefficients significantly below these values, close to the values predicted by a linear extension of the data from Walter (1998).

Overall, the increased partition coefficients seen in the pyroxenite melting experiments should not be unexpected. Melting of a pyroxenite at gradually lower *T* produces liquids that are enriched in silica and deficient in FeO and MgO relative to melting of peridotite (Pertermann and Hirschmann, 2003). Because FeO, MgO, and MnO decrease with increasing silica in the liquid, the partition coefficients increase accordingly. At *T* above 1525°C, the pyroxenites examined by Pertermann and Hirschmann (2003) are above their liquidus. While our experiments show a slight enrichment in $SiO_2$ due to their hydrous nature (Chapter 2), the enrichment is much less than that seen during pyroxenite melting. In peridotite melting, the presence of olivine buffers the MgO, FeO, MnO, and $SiO_2$ contents of the liquid within a much narrower range. Our experiments therefore show a lower partition coefficient for each element. Notably, the partition coefficients for each element change at different rates; $D_{MgO}$ increases more with decreasing *T* than $D_{MnO}$, and $D_{MnO}$ increases slightly more with

decreasing $T$ than $D_{FeO}$, suggesting that pyroxenite melting near the solidus may be able to fractionate FeO and MnO.

Very few measurements of the partitioning of these elements between liquids and orthopyroxenes exist in this $T$ range. Some experiments of Walter (1998) do include orthopyroxene as a phase and possibly define trends of variation with $T$ as seen for other solids. Where they are reported by Walter (1998), the partition coefficients $D_{FeO}$ and $D_{MnO}$ for orthopyroxene are not significantly different from those measured in clinopyroxene. While it is possible that the behavior of the two pyroxenes could differ strongly at lower $T$ during hydrous melting, there is no suggestion of that in the experiments of Walter (1998).

**4.3 MnO partitioning in garnet**

Prior to this work, measurements of the partitioning of MnO between garnet and liquid at 3 GPa were limited, and partitioning measurements involving hydrous melts at this $P$ were non-existent. The work of Walter (1998) reported measurements of MnO partitioning from pressures greater than 3 GPa, but no single experiment at 3 GPa gives compositional measurements for both garnet and liquid. At higher $P$, measurements of both phases are given and thus partition coefficients can be calculated, but those partition coefficients differ significantly from the ones reported here. In contrast to the olivines and the pyroxenes, $T$ dependence is not able to explain the difference in garnet/melt partitioning between the current experiments and those of Walter (1998) despite a well-defined relationship between $D_{MnO}^{garnet/melt}$ and $T$ among Walter (1998)'s data (Figure 3). Our samples show both FeO and particularly MnO to be noticeably more compatible in garnet at this $T$ than predicted by the trends defined by the experiments of Walter (1998).

Garnet is therefore the only phase for which $D_{MnO}$ and $D_{FeO}$ could not be approximated by linear extrapolation in *T* from the experiments of Walter (1998).

There are several causes of the stark differences in measured partition coefficients at a constant *T*. One obvious explanation would be that there was a major difference in the composition of the garnets between our samples in equilibrium with hydrous liquids and the experiments in equilibrium with anhydrous melts, as is discussed for cpx in Chapter 2. However, the differences in composition between the garnets from the two sets of experiments appear minor at best. Table 2 shows an analysis for a 3 GPa garnet given by Walter (1998) and a representative garnet composition from one of our experiments, and in general the compositions are similar. $Cr_2O_3$ and $TiO_2$ are measurably higher in the garnets from Walter (1998), but it seems unlikely that these minor components, whose cations substitute in garnet on a different crystallographic site than MnO, should strongly influence the $D_{MnO}^{garnet/melt}$. The major difference appears to be that the garnets in these experiments have a higher Mg#. This could relate to a number of factors. In the experiments of Walter (1998), the Mg# in garnet decreases with decreasing *T* at each constant *P*, and therefore the lower Mg# in our garnets is not unexpected. However, this temperature-trend is not nearly sufficient to fully explain the difference in measured (Figure 3).

A second possible explanation for the variation in partition coefficients is changes in oxygen fugacity. If our experiments were performed under considerably more oxidizing conditions and $Mn^{3+}$ were more compatible in garnet, then $fO_2$ could provide an explanation for the variation in apparent $D_{MnO}^{garnet/melt}$. The MnO-$Mn_3O_4$ buffer should sit at an oxygen fugacity 4 log units above the QFM buffer at this *T* (Berndt et al., 2004).

This fact suggests that very oxidizing conditions must be imposed for $Mn_3O_4$ to become a factor. The experiments of Walter (1998), Longhi (2002), and Pertermann and Hirschmann (2003) were all performed in graphite capsules, which would be expected to fix the oxygen fugacity of the sample at the C-CO buffer. Our experiments were designed to stay close to two log units below the QFM buffer, which should be a realistic value for the current mantle. While they are not buffered by the presence of a specific phase, a strong buffer may be maintained by the pre-saturation of the capsules. As shown in Chapter 4 of this thesis and by Kessel et al. (2001), the Fe contents of Au/Pd and Pt capsules in equilibrium with silicate liquids are strong functions of $fO_2$. Thus, a large change in $fO_2$ would require a large change in the Fe content of the capsules and of the experiments themselves, which is not seen (although some variation in the Fe content does occur). Furthermore, the olivine-liquid exchange parameter $K_D$ provides an additional check on our oxygen fugacity constraints; conditions that were too oxidizing would be expected to produce liquids with a higher total iron content than predicted by the calibrated $K_D$ parameter due to the uptake of iron from the capsules. Our experiments best fit the predicted $K_D$ parameter under reducing conditions, approximately 2 log units below the QFM buffer, close to where the liquids were originally set. Higher oxygen fugacities would result in more Mg-rich olivines than we measure at this iron content. The C-CO buffer is approximately 4 log units below the QFM buffer at this $T$ and $P$ (e.g., Frost and Wood, 1995), suggesting that our experiments likely show only slight increases in oxidized Fe and even less in Mn compared with the other experiments considered here, a conclusion consistent with the $K_D$ relations. The consistent trend in partition

coefficients for olivine described above also argues that there is no major change in the oxidation state of Mn between the different sets of experiments.

As the experiments of Walter (1998) do not include a measurement of both garnet and liquid compositions from a single experiment at 3GPa, but only from a higher *P*, it seems plausible that there may be a significant *P* effect on the partitioning of these elements beginning between 3 and 4 GPa, although that would be unexpected. One way of confirming this could be investigation of MnO partitioning from other melting experiments from similar *P*. Longhi (2002) reported measurements of garnet and liquid compositions in anhydrous melting experiments from 2.8 GPa, and the partitioning of FeO is similar to the experiments of Walter (1998). In these same experiments, however, MnO is observed to be more compatible in garnet than in the experiments of Walter (1998), with reported partition coefficients varying between 1.2 and 1.7. A more precise calculation of MnO partitioning from the data reported by Longhi (2002) is difficult because of the high standard deviation on analyses for MnO in that study. Johnson (1986) also conducted melting experiments in a similar *P* and *T* range on basalts with high $Al_2O_3$ contents and measured elevated partition coefficients for MnO in garnets as well. While no obvious *T* or *P* correlation could be observed from that data, $D_{MnO}^{garnet/melt}$ at 1500 °C and 3GPa was measured to be ~1.6 and values up to 5.85 were measured at 1400 °C and 3 GPa. Finally, the experiments of Pertermann and Hirschmann (2003) at *P* from 2 to 3 GPa and temperatures from 1250 °C to 1375 °C showed $D_{MnO}^{garnet/melt}$ values from 3.1 to 4.9, with values at 3 GPa forming a trend versus *T* that does not form a consistent relationship with either our experiments or those from Walter (1998) (Figure 3). From the available experiments, no clear *P* dependence can be determined, although every experiment at 3

GPa and below, other than those of Walter (1998), shows $D_{MnO}^{garnet/melt}$>1.0. This does suggest that pressure-sensitivity may increase with decreasing *P*. When $D_{MnO}^{garnet/melt}$ is plotted against $D_{FeO}^{garnet/melt}$ or $D_{MgO}^{garnet/melt}$, which presumably have similar interactions with the liquid, straight lines are found (Figure 3). The slopes of these lines differ from unity, such that the ratios of partition coefficients do change with changing *T* and liquid compositions. Hence, changes in relative partitioning are possible under differing melting conditions. Overall, the general trend in all of the experiments, including those at lower *T*, is for $D_{MnO}^{garnet/melt}$ to increase faster than $D_{FeO}^{garnet/melt}$ as *T* decreases, leading to stronger fractionation at lower *T*.

While none of these explanations appear satisfactory on their own, each potentially plays at least a small role in the variation of $D_{MnO}^{garnet/melt}$ at constant *T* seen in our experiments. Based on the increase in $D_{MnO}^{garnet/melt}$ at still lower *T*, it appears that the effect of low *T* on the $D_{MnO}^{garnet/melt}$ may be particularly important. While it remains surprising that the experiments of Walter (1998), which cover a range of several hundred degrees in *T*, do not show variation of the magnitude observed here, it is possible that the variation in $D_{MnO}^{garnet/melt}$ becomes much more extreme and non-linear at lower temperatures or in different liquid compositions. The unexpected $D_{MnO}^{garnet/melt}$ in this work argues that experimental calibration across a much wider range of *T*, *P*, $fO_2$, and liquid composition is a prerequisite for understanding the global variation in Fe/Mn ratios in natural liquids. However, the pressures and compositions examined in the studies cited here do give us the ability to evaluate the plausible range of liquid compositions that could be produced

by natural melting from peridotites, pyroxenites, and hydrous peridotites, and therefore to make inferences about the production of natural melts.

4.3.1 Lattice strain partitioning model

Based on lattice strain calculations, Van Westrenen et al. (2001) produced a model for the partitioning of cations into garnet that allowed for predictive calculation of the solid/liquid partition coefficient for a number of elements, including Fe, Mg, and Mn. We performed a similar calculation using their model to try to fit the series of partition coefficients measured here, and the results suggest that, in this case, the liquid appears to exert an important control on the partitioning for all 3 elements.

In the lattice strain model of Van Westrenen et al. (2001), the elements with the greatest *D* will be those that fit into the available site with the least distortion of the lattice based on their ionic radii, and a plot of the ionic radius of each element versus the partition coefficient should be approximately parabolic. The ionic radius (*r*) of the divalent cations in the appropriate coordination for the X-site of garnet is $r_{Mn} > r_{Fe} > r_{Mg}$, such that either $D_{FeO}^{garnet/melt}$ should be greater than both $D_{MnO}^{garnet/melt}$ and $D_{MgO}^{garnet/melt}$ if Fe fits best into the garnet structure, or there should be a consistent pattern where the partition coefficients either decrease or increase in the same order as the ionic radius. Our results and the results of Walter (1998) both show a trend that is not predicted by this lattice-strain model as both sets of experiments show $D_{MnO}^{garnet/melt}$ and $D_{MgO}^{garnet/melt}$ greater than $D_{FeO}^{garnet/melt}$.

Using the lattice-strain formalism of Van Westrenen et al. (2001), we derived a fit to predict $D_{MnO}^{garnet/melt}$ based on a measured value of $D_{MgO}^{garnet/melt}$ (Figure 4) and calibrated by

varying $r_0$, the size of the lattice site on which these elements sit, to fit both $D_{MgO}^{garnet/melt}$ and $D_{MnO}^{garnet/melt}$. We performed a similar fit for experiment 40.06 at 4 GPa and 1590 °C from Walter (1998). In both cases, the value for $r_0$ of 2+ cations is smaller than that expected from the expressions in Van Westrenen et al. (2001) but probably this difference is within the uncertainty in both calibrations. However, in both our own experiments and those of Walter (1998), we are unable to fit the value of $D_{FeO}^{garnet/melt}$ and $D_{MnO}^{garnet/melt}$ simultaneously as functions of $D_{MgO}^{garnet/melt}$ (Figure 4). We can produce a fit to $D_{FeO}^{garnet/melt}$ based on the same model (Figure 4b) but it requires more extreme values of $r_0$ outside the range fit by Van Westrenen et al. (2001) and fails to fit the MnO data from the same experiments. We conclude that FeO, a major component of both garnet and melt, is probably not behaving like a trace element in a simple Henrian manner and fuller consideration of garnet and melt thermodynamics are required to explain the observations for this oxide.

**4.4. Bulk partitioning calculations**

Our measurements of mineral/melt partitioning of MnO and FeO allow the calculation of bulk partition coefficients and therefore we can estimate liquid compositions in equilibrium with a given solid assemblage. This particular set of partition coefficients produces a rich variety of melting behavior when small changes in the mineralogy of the melting source are considered. The MnO content of liquids are a strong function of the modal abundance of garnet. Conversely, the FeO content of a liquid is a strong function of the modal olivine/pyroxene ratio, because of iron's compatibility in olivine and incompatibility in either pyroxene. The FeO/MnO ratio of any liquid

produced, therefore, is a very strong function of the ratio of olivine to garnet in the source.

Qin and Humayun (2008) produced a large quantity of whole-rock Fe/Mn measurements that likely span much of the global variation in this parameter (for convenience, we plot FeO*/MnO here; the difference between these two parameters should be 0.3%). The Fe/Mn ratio for their available terrestrial database varied from ~53 to ~70, with depleted Atlantic Ocean MORB at the low end and Hawaii and Tahiti at the high end. If these represent the end-members for typical terrestrial basalts, this range can be understood from the partition coefficients given here and reasonable variations of the source material.

Our melting experiments were performed using a starting material recrystallized from fertile peridotite KLB-1 as discussed in Chapter 2. The composition of KLB-1 was measured by Davis et al. (2009) to have 8.2% FeO and 0.12% MnO. This gives an FeO/MnO ratio of 68 in the starting peridotite. The expected mode of KLB-1 in the garnet stability field is about 60% olivine, 30% cpx, and 10% garnet (Chapter 2). Melting of this starting material with its high olivine content will produce a liquid with a lower FeO/MnO ratio than the source because of the high $D_{FeO}^{olivine/melt}$. Our final liquid composition gives an FeO/MnO ratio of 59. This value is very internally consistent with the calculated composition of a low-degree melt of this source (also ~59).

Figure 5 shows ternary diagrams giving the estimated FeO/MnO ratio in a liquid generated by batch melting of a source with an assigned initial FeO/MnO ratio and assigned partition coefficients based on this work. As discussed above, the orthopyroxene and clinopyroxene appear to have similar FeO and MnO partitioning under the melting

conditions considered here. Neither FeO nor MnO is strongly compatible in either phase, and so their capacity to fractionate these oxides is limited and they will be considered together in this analysis. We estimate that variations in orthopyroxene and cpx ratio yield less than 2 units in FeO/MnO ratio, except in lithologies that are almost pure pyroxene, where it can be up to 5 units between the pure orthopyroxene and cpx end-members. We calculate the liquid FeO/MnO ratio solely using the batch melting equation and as such we do not explicitly consider large shifts in mineralogy due to non-modal melting reactions, although some insights may still be gained into that process by considering the change in the modal mineralogy of the residue during melting.

Using the recommended FeO/MnO ratio of KLB-1 (i.e. 68) as a starting point, melting of a fertile, olivine-rich peridotite similar to KLB-1 gives FeO/MnO ratios ~55-60. These values are consistent with the measurements of Qin and Humayun (2008) for MORB. Melting of a more depleted, olivine-rich source with the same initial FeO/MnO ratio produces basalts with lower FeO/MnO ratios. Production of Atlantic-type MORB by melting of a source with the same FeO/MnO ratio as KLB-1 requires a higher olivine fraction in the source, ~70% modal olivine. Using a constant value of the modal abundance of pyroxene of 20%, an FeO/MnO ratio of 53 in the equilibrium basalt occurs with a modal abundance of 75% olivine and 5% garnet. This high olivine content would be consistent with a low-aluminum, depleted source. Variation in the amount of pyroxene has only a limited effect on the calculated FeO/MnO – an 80% olivine, 10% pyroxene, 10% garnet source produces the same FeO/MnO ratio.

Low-degree melting of a more fertile source, with lower olivine content, produces liquids with a higher FeO/MnO ratio at these temperatures. Melting of this peridotite

under these conditions is expected to produce liquids with FeO/MnO close to 60 and ~0.14% total MnO. These values are, unsurprisingly, very close to the values produced in our experiments, and are more typical of the melting that produces Pacific-type MORB (Qin and Humayun, 2008).

Continued enrichment of the melting source is expected to continue to decrease the olivine modal abundance relative to garnet and pyroxenes. Thus, melting of a more enriched source material with the same initial FeO/MnO ratio at these temperatures would be expected to produce melts with increased FeO/MnO ratios. Considering only the variation in the garnet to olivine ratio under these conditions, a liquid with FeO/MnO of 70 would be produced when the garnet to olivine ratio is ~0.75. This theoretical high-garnet peridotite composed of minerals with our measured compositions would have a high-aluminum content compared to KLB-1, about 7.5% compared with 3.51% in the natural version (Davis et al., 2009). While this composition is rare, it is similar to some peridotites that have been sampled, such as in the Red Sea rift (e.g., Bonatti et al., 1986). Compared to typical mantle, this type of peridotite would be more enriched and may represent a metasomatic product or the product of the addition of a highly aluminous material, such as subducted sediment, to normal mantle. Increasing the modal abundance of pyroxene in the calculation allows us to produce a melt with a FeO/MnO ratio of ~70 with a lower alumina content, because it takes less garnet to alter that ratio. Thus, increasing the CaO, $Al_2O_3$, or $SiO_2$ content of a peridotite by addition of enriched or recycled material has the ability to produce high FeO/MnO ratios through the melting process without significant involvement of either an iron-rich or a manganese-rich component. Because we can now postulate a new mechanism for the variation of

FeO/MnO occurring solely within the melting column that could produce variations much larger than those seen in terrestrial basalts, we conclude that on its own, changes in FeO/MnO within or between suites of basalts cannot on its own be taken as evidence for core-mantle interaction. The complex melting process may obscure any signals of core-derived material unless the modal mineralogy of the source is very well known.

An important additional consideration must be the initial FeO/MnO ratio of any material added to normal peridotite. However, the available measurements and our data provide constraints on this as well. As noted by Qin and Humayun (2008), most of the common MORB have bulk FeO/MnO ratios between 50 and 60. These numbers are consistent with our calculations of the FeO/MnO ratios that would be produced by low-degree melting of a typical peridotite. If the FeO/MnO ratio is not disturbed by subduction-related processing, then eclogitic sources formed from subducted oceanic crust and gabbroic lower crust could be expected to start with FeO/MnO ratios in this range. Notably, most pyroxenitic or eclogitic materials used by other authors fall in this range as well. The pyroxenite compositions of Pertermann and Hirschmann (2003) are 49 (G2) and 57 (G2K). Johnson (1986) used high-alumina natural basalts with ratios of 48 and 36 and MORB samples with ratios of 58, 61, and 93 (with some possible analytical error on the low MnO concentration). Yaxley and Green (1998) used starting material with a ratio of 58. Takahashi and Nakajima (2002) used an Archean MORB with a ratio of 56, a normal MORB at 56, a sample from Iceland at 59, and a Columbia River basalt at 68. All of these experimental pyroxenite compositions, together with the global basalt survey of Qin and Humayun (2008), suggest that an FeO/MnO ratio of 55 is an adequate

estimate for pyroxenitic source components, although more extreme values may be possible.

Direct melting of a rock with an initial FeO/MnO ratio of 55 and our partition coefficients gives the triangle in Figure 5b. As long as the modal mineralogy remains composed of a mixture of pyroxene and garnet, the FeO/MnO ratio of the liquid produced is significantly greater than that of the source. The calculation in 5b assumes a high degree of melting (50%); a lower degree of melting produces even higher final ratios. We can also repeat this calculation using the partition coefficients for garnet and pyroxene from the pyroxenite melting experiments of Pertermann and Hirschmann (2003). Since the ratio $D_{FeO}/D_{MnO}$ is lower in those experiments than in the experiments of Walter (1998), using their partition coefficients increases the FeO/MnO ratio in the calculated liquid (Figure 5c). In fact, every liquid composition reported in that work gives an FeO/MnO ratio over 90 except for the samples from the highest *T*, where the partition coefficients approach the values of Walter (1998) and very little garnet or clinopyroxene remain in the source.

Sobolev et al. (2007) and Gurenko et al. (2009) presented a model for the calculation of the source of melting based in part on the measured FeO/MnO ratio of olivines crystallized from liquids. In their model, elevated FeO/MnO ratios are produced by the melting of an olivine-free source created by interaction of peridotite with a high-silica melt derived by high-degree melting of upwelling recycled oceanic crust. Our derived mineral-melt partition coefficients provide a possible test of that hypothesis and the conditions under which it could be applicable. As shown above, high-degree melting of a recycled eclogite or pyroxenite source will produce liquids that have high FeO/MnO

ratios, higher than low-degree melts of peridotite even though the eclogite or pyroxenite source may have a lower FeO/MnO ratio than a typical peridotite source. If typical upper mantle can be adequately represented by KLB-1 (an assumption supported by the global range in FeO/MnO ratios in MORB seen by Qin and Humayun, 2008), then adding a high-degree melt of an eclogitic or pyroxenitic source will not decrease the FeO/MnO ratio of the starting peridotite. Therefore, the FeO/MnO ratio of the "reaction pyroxenite" produced can only be increased by the process of refertilization. This source would be olivine-free and would therefore contain a mixture of pyroxenes and garnet. Partial melting of this lithology would then be expected to produce basalts with very high FeO/MnO contents, even if melted to high degree (Figure 5d). Using estimates of the degree of melting similar to those in Sobolev et al. (2007), the FeO/MnO ratio of the melt of the reaction pyroxenite would be ~80. While this is higher than the average Hawaiian value of ~68-70, mixing of this liquid with a peridotite-derived liquid could bring the erupted final FeO/MnO ratio down. Sobolev et al. (2007) proposed that some Hawaiian volcanoes show 60-70% melts of pyroxenite in their sources, and those values are consistent with the mixing relations calculated here. In cases of nearly complete melts of pyroxenite, as proposed for Siberia (Sobolev et al., 2009) or the Canary Islands (Gurenko et al., 2009), this model predicts very elevated whole rock FeO/MnO contents. As above, utilizing the partition coefficients from Pertermann and Hirschmann (2003), even from their highest *T* measurement, only increases the FeO/MnO of the estimated pyroxenite melt and thus would require a reduction in the pyroxenite component in the source. In this case, the partition coefficients measured on peridotites in the study of Walter (1998) appear to better fit the Sobolev et al. (2007) model than the partition coefficients

measured on pyroxenites by Pertermann and Hirschmann (2003), suggesting that this model can only produce the measured FeO/MnO ratios during melting at *T* higher than expected in normal mantle.

The Sobolev et al. (2007) model also incorporated a number of additional elements on which we have more limited constraints. In particular, their model also incorporates nickel abundances in olivine; an element about which our experiments give no information because nickel is strongly compatible in our capsule material and is at or below the detection limit of our analyses. Furthermore, we note that our partitioning data only has limited applicability to Hawaii and Iceland, because of the estimated higher *T* at the site of melting. However, based on Figure 5(c) we can note that production of the elevated FeO/MnO signature in Hawaii or Tahiti by melting of a pyroxene and garnet rich source at low temperature will produce liquids with much greater FeO/MnO than are observed in the global synthesis of Qin and Humayun (2008), and mixing of these melts with low degree melts of peridotite would be unable to dilute this signal. While this calculation is idealized, it reinforces our statement that a full accounting of the partitioning of MnO must be completed before using MnO as a method of determining source abundances, as MnO compatibility in garnet can produce large shifts in the calculated source makeup.

**4.6. Other implications**

The effects on $D_{\mathrm{MnO}}$ observed here, in particular the increased $D_{MnO}^{garnet/melt}$ during hydrous melting may have other implications for global magmatism. During melting of peridotite under a mid-ocean ridge, much of the volume of melt is produced in the spinel peridotite field regardless of the water content. Thus, the melt produced by low-degree,

hydrous melting in the garnet field may be a component that is overprinted by later high-degree melting or by shallow-level fractional crystallization, which has also been shown to alter the FeO/MnO ratio (Qin and Humayun, 2008). One mechanism for possibly isolating the presence of hydrous melts from the garnet facies may be to look for correlations between FeO/MnO and other indices that suggest the presence of garnet during melting, such as high-precision measurement of Dy/Yb (e.g., Salters and Longhi, 1999). In Figure 5 we show a selection of data from Hildenbrand et al. (2008) from the Azores. These samples are whole rock measurements from a selection of their data filtered for effects of extensive fractional crystallization using La abundances, including high-precision MnO analyses. In these samples, whole rock Dy/Yb does appear to be correlated with whole rock FeO/MnO. Unfortunately, very few other data sets currently can be evaluated in this way, because very few give precise data on MnO concentrations at the level where small changes in FeO/MnO ratio could be treated as significant. This result suggests that interpreting the FeO/MnO variation during melting may require both high-precision analyses of MnO and simultaneous analyses of the trace element compositions, as both may give information on the presence and behavior of garnet during melting.

## 5. CONCLUSION

During hydrous melting in the garnet field, MnO is more compatible in garnet than would be predicted by previous experiments. FeO is compatible in olivine, and thus, varying amounts of olivine and garnet in a melting source are able to fractionate MnO from FeO during melting. Hydrous melting experiments on a peridotite close in composition to KLB-1 produces melts with a FeO/MnO ratio similar to that measured in

normal mid-ocean ridge basalt. Melting of a source with lower olivine content and higher garnet content can produce fractionations that are larger than the globally observed variation in this ratio. Hydrous melting in the presence of garnet may produce correlations between the FeO/MnO ratio and other indices indicative of the presence of garnet in the melting source.

## 6. ACKNOWLEDGEMENTS

The authors would like to thank Andrew Matzen and Mike Baker for illuminating discussions regarding the behavior and analysis of MnO in experiments. This work was supported by the NSF Ocean Sciences Marine Geology and Geophysics program, grant numbers OCE-0241716 and OCE-0550216.

**References**

Berndt, J., Koepke, J., and Holtz, F. (2005) An experimental investigation of the influence of water and oxygen fugacity on differentiation of MORB at 200 MPa. *J. Petrol.* **46**, 135-167.

Brady, J. B. and McCallister, R. H. (1983) Diffusion data for clinopyroxenes from homogenization and self-diffusion experiments. *Am. Mineral.* **68**, 95-105.

Bonatti, E., Ottonello, G., and Hamlyn, P. R., (1986) Peridotites from the island of Zabargad (St. John), Red Sea: petrology and geochemistry. *J. Geophys. Res.* **91**, 599-632.

Cherniak, D. J. (2001) Pb diffusion in Cr diopside, augite, and enstatite, and consideration of the dependence of cation diffusion in pyroxene on oxygen fugacity. *Chem. Geol.* **177**, 381-397.

Davis, F. A., Tangeman, J. A., Tenner, T. J., and Hirschmann, M. M. (2009) The composition of KLB-1 peridotite. *Am. Mineral.* **94**, 176-180.

Dixon, J. E., Stolper, E. M., and Holloway, J. R. (1995) An experimental study of water and carbon dioxide solubilities in mid ocean ridge basaltic liquids.1. Calibration and solubility models. *J. Petrol.* **36**, 1607-1631.

Frost, D. and Wood, B. (1995) Experimental measurements of the graphite C−O equilibrium and $CO_2$ fugacities at high temperature and pressure. *Contrib. Mineral.Petr.* **121**, 303-308.

Gaetani, G. A. and Grove, T. L. (1998) The influence of water on melting of mantle peridotite. *Contrib. Mineral. Petr.* **131**, 323-346.

Gurenko, A. A., Sobolev, A. V., Hoernle, K. A., Hauff, F., and Schmincke, H.-U. (2009) Enriched, HIMU-type peridotite and depleted recycled pyroxenite in the Canary plume: A mixed-up mantle. *Earth Planet Sc. Lett.* **277**, 514-524.

Hildenbrand, A., Madureira, P., Marques, F. O., Cruz, I., Henry, B., and Silva, P. (2008) Multi-stage evolution of a sub-aerial volcanic ridge over the last 1.3 Myr: S. Jorge Island, Azores Triple Junction. *Earth Planet Sc. Lett.* **273**, 289-298.

Johnson, A. D. (1986) Anhydrous P-T phase relations of near-primary high-alumina basalt from the South Sandwich Islands. Implications for the origin of island arcs and tonalite-trondjemite series rocks. *Contrib. Mineral. Petr.* **92**, 368-382.

Kessel, R., Beckett, J. R., and Stolper, E. M. (2001) Thermodynamic properties of the Pt-Fe system. *Am. Mineral.* **86**, 1003-1014.

Longhi, J. (2002) Some phase equilibrium systematics of lherzolite melting: I. *Geochem. Geophys. Geosyst.* **3**, 1020.

Mysen, B. O., Virgo, D., Harrison, W. J., and Scarfe, C. M. (1980) Solubility mechanism of $H_2O$ in silicate melts at high pressures and temperatures: a Raman spectroscopic study. *Am. Mineral.* **65**, 900-914.

Qin, L. and Humayun, M. (2008. The Fe/Mn ratio in MORB and OIB determined by ICP-MS. *Geochim Cosmochim Ac.* **72**, 1660-1677.

Ohlhorst, S., Behrens, H., and Holtz, F. (2001) Compositional dependence of molar absorptivities of near-infrared $OH^-$ and $H_2O$ bands in rhyolitic to basaltic glasses. *Chem. Geol.* **174**, 5-20.

Patino-Douce, A. E. (2005) Vapor-Absent Melting of Tonalite at 15-32 kbar. *J. Petrol.* **46**, 275-290.

Pertermann, M. and Hirschmann, M. M. (2003) Anhydrous partial melting experiments on MORB-like eclogite: phase relations, phase compositions and mineral-melt partitioning of major elements at 2-3 GPa. *J. Petrol.* **44**, 2173-2201.

Putirka, K. D. (2005) Mantle potential temperatures at Hawaii, Iceland, and the mid-ocean ridge system, as inferred from olivine phenocrysts: evidence for thermally driven mantle plumes. *Geochem. Geophys. Geosyst.* **6**, Q05L08.

Salters, V. J. M. and Longhi, J. (1999) Trace element partitioning during the initial stages of melting beneath mid-ocean ridges. *Earth Planet Sc. Lett.* **166**, 15-30.

Sobolev, A. V., Hofmann, A. W., Kuzmin, D. V., Yaxley, G. M., Arndt, N. T., Chung, S.-L., Danyushevsky, L. V., Elliott, T., Frey, F. A., Garcia, M. O., Gurenko, A. A., Kamenetsky, V. S., Kerr, A. C., Krivolutskaya, N. A., Matvienkov, V. V., Nikogosian, I. K., Rocholl, A., Sigurdsson, I. A., Sushchevskaya, N. M., and Teklay, M. (2007) The amount of recycled crust in sources of mantle-derived melts. *Science* **316**, 412-417.

Sobolev, A., Krivolutskaya, N., and Kuzmin, D. (2009) Petrology of the parental melts and mantle sources of Siberian trap magmatism. *Petrology* **17**, 253-286.

Takahashi, E. and Nakajima, K. (2002) Melting processes in the Hawaiian plume: an experimental study. In: Lipman, P. W., Garcia, M. O., Naka, J., and Aramake, S. Eds.) *Hawaiian Volcanoes: Deep Underwater Perspectives. Geophys. Mono.* American Geophysical Union, **128**, 403-418.

Toplis, M. J. (2005) The thermodynamics of iron and magnesium partitioning between olivine and liquid: criteria for assessing and predicting equilibrium in natural and experimental systems. *Contrib. Mineral. Petr.* **149**, 22-39.

Walter, M. J. (1998) Melting of garnet peridotite and the origin of komatiite and depleted lithosphere. *J. Petrol.* **39**, 29-60.

Wang, Z. and Gaetani, G. A. (2008) Partitioning of Ni between olivine and siliceous eclogite partial melt: experimental constraints on the mantle source of Hawaiian basalts. *Contrib. Mineral. Petr.* **156**, 661-678.

Van Westrenen, W., Allan, N. L., Blundy, J. D., Purton, J. A., and Wood, B. J. (2000) Atomistic simulation of trace element incorporation into garnets-comparison with experimental garnet-melt partitioning data. *Geochim. Cosmochim. Ac.* **64**, 1629-1639.

Yaxley, G. and Green, D. (1998) Reactions between eclogite and peridotite: Mantle refertilisation by subduction of oceanic crust. *Schweizerische mineralogische und petrographische Mitteilungen* **78**, 243-255.

**TABLES**

Table 1

| | $D_{MnO}$ | $D_{FeO*}$ | $D_{MgO}$ | $K_D$ |
|---|---|---|---|---|
| Clinopyroxenes | | | | |
| R385 | 0.67 | 0.47 | 1.29 | |
| R389 | 0.71 | 0.56 | 1.30 | |
| R390 | 0.66 | 0.43 | 1.31 | |
| R393 | 0.73 | 0.49 | 1.36 | |
| R395 | 0.71 | 0.56 | 1.32 | |
| R396 | 0.73 | 0.53 | 1.30 | |
| R398 | 0.73 | 0.50 | 1.27 | |
| Garnets | | | | |
| R385 | 1.55 | 1.00 | 1.45 | |
| R389 | 1.48 | 1.12 | 1.39 | |
| R390 | 1.53 | 1.04 | 1.28 | |
| R393 | 1.55 | 0.92 | 1.44 | |
| R395 | 1.48 | 1.12 | 1.36 | |
| R396 | 1.56 | 0.94 | 1.46 | |
| R398 | 1.43 | 0.96 | 1.39 | |
| Olivines | | | | |
| R385 | 0.85 | 1.22 | 3.56 | 0.350 |
| R389 | 0.83 | 1.32 | 3.44 | 0.399 |
| R390 | 0.85 | 1.19 | 3.50 | 0.339 |
| R393 | 0.81 | 1.20 | 3.54 | 0.362 |
| R395 | 0.83 | 1.32 | 3.40 | 0.383 |
| R396 | 0.85 | 1.24 | 3.46 | 0.360 |
| R398 | 0.76 | 1.11 | 3.39 | 0.328 |
| Liquid FeO/MnO | | | | |
| R385 | 60.3 | | | |
| R389 | 51.8 | | | |
| R390 | 62.7 | | | |
| R393 | 59.4 | | | |
| R395 | 49.6 | | | |
| R396 | 59.0 | | | |
| R398 | 54.4 | | | |

Table 1: Experimental data used in this study from samples where MnO contents were measured using high-precision techniques. Remaining oxides are presented in Chapter 2.

Table 2

| | Walter, 1998 | This work |
|---|---|---|
| Run: | 30.05 | R396 |
| $SiO_2$ | 42.42 | 41.91 |
| $TiO_2$ | 0.53 | 0.18 |
| $Cr_2O_3$ | 1.53 | 0.80 |
| $Al_2O_3$ | 22.2 | 23.01 |
| FeO | 6.22 | 8.14 |
| MgO | 21.81 | 20.43 |
| CaO | 5.43 | 6.26 |
| MnO | 0.2 | 0.23 |
| $Na_2O$ | 0.03 | 0.02 |
| Total | 100.37 | 100.99 |
| Mg# | 86.2 | 81.73 |

Table 2: Measured 3 GPa garnet compositions from Walter (1998) and from this work. Experiment 30.05 was conducted at 1500°C, but no liquid composition was reported so a full partition coefficient could not be explicitly calculated.

**FIGURE CAPTIONS**

Figure 1. Measured values of mineral-melt partition coefficients for olivine from this work (triangles), Walter (1998) (squares), and basalts from Wang and Gaetani (2008) (circles). The trend in Figure 1c is linear, and the lack of linearity in the other figures can be understood using the relationships between liquid composition, *T*, and $K_D$ calibrated by Toplis (2005).

Figure 2. Measured values of the mineral/melt partition coefficients for clinopyroxene from this work (triangles), Walter (1998) (squares), and Pertermann and Hirschmann (2003) (blue diamonds). Cpx from our experiments overlap the partition coefficients from Walter (1998) despite much lower *T*. The values from Pertermann and Hirschmann (2003) diverge substantially, and imply increasing compatibility of the oxides with decreasing *T*. The highest T experiment of Pertermann and Hirschmann (2003) is approaching its liquidus at 3GPa and also approaches the partition coefficients measured by Walter (1998) at similar *T*.

Figure 3. Measured partition coefficients for garnet. Symbols as in Figure 2. Arrow in Figure 3a points towards remaining experiments from Pertermann and Hirschmann (2003); we adjusted our scale in this image to best illustrate the relationship between our measured partition coefficients and the trend of Walter (1998) (black line). Our values for $D_{MnO}^{garnet/melt}$ are significantly above the trend predicted based on extrapolation in *T* from Walter (1998). They are also substantially below the values measured during pyroxenite melting by Pertermann and Hirschmann (2003) at the same *T*.

Figure 4. Garnet/melt partition coefficients fit to a lattice-strain model of the form of Van Westrenen et al. (2001). Filled circles are average partition coefficients from this work, open circles are measured partition coefficients from experiment 40.06 from Walter (1998). Solid lines represent calculated partition coefficients based on the measurement of $D_{MgO}^{garnet/melt}$ and dashed lines represent calculated partition coefficients based on the same experiment from Walter (1998), both fit to a model of the form of Van Westrenen et al. (2001). In Figure 4a, a value of 0.9225Å for the parameter $r_0$ is used for the solid line and a value of 0.929Å for the parameter $r_0$ is used for the dashed line. In Figure 4b a value of 0.88Å for the parameter $r_0$ is used for the solid line and a value of 0.87Å for the parameter $r_0$ is used for the dashed line. In both cases we are unable to produce a curve that fits both the values of $D_{MnO}^{garnet/melt}$ and $D_{FeO}^{garnet/melt}$ simultaneously based on a measured value of $D_{MgO}^{garnet/melt}$.

Figure 5. Calculated melt FeO/MnO ratios as discussed in the text, plotted for a fixed FeO/MnO ratio in the source and variable mineralogies. 5(a) 1% melt of peridotite with the FeO/MnO ratio of KLB-1 given by Davis et al. (2009) gives similar results to the liquids measured in our experiments. 5(b) The melts that would be produced by 50% melting of a source with an initial FeO/MnO = 55, simulating melting of recycled material. 5(c) The same melt scenario in 5(b), but using the partition coefficients measured at 1375 °C by Pertermann and Hirschmann (2003), giving much higher values of FeO/MnO for any pyroxene-rich source. 5(d) The liquids that would be produced by

melting of an approximate “reaction pyroxenite” as hypothesized by Sobolev et al. (2007) using the measured partition coefficients from this work.

Figure 6. Whole rock Dy/Yb versus FeO/MnO for selected samples from Hildenbrand et al. (2008), from the Azores. Samples displayed here were selected based on the criteria used by these authors to distinguish increasing amounts of differentiation from processes occurring in the melting source region. Curve represents a mixing hyperbola calculated using end-members just outside of the data range. Error bars are estimated based on the reported precision in that work.

**FIGURES**

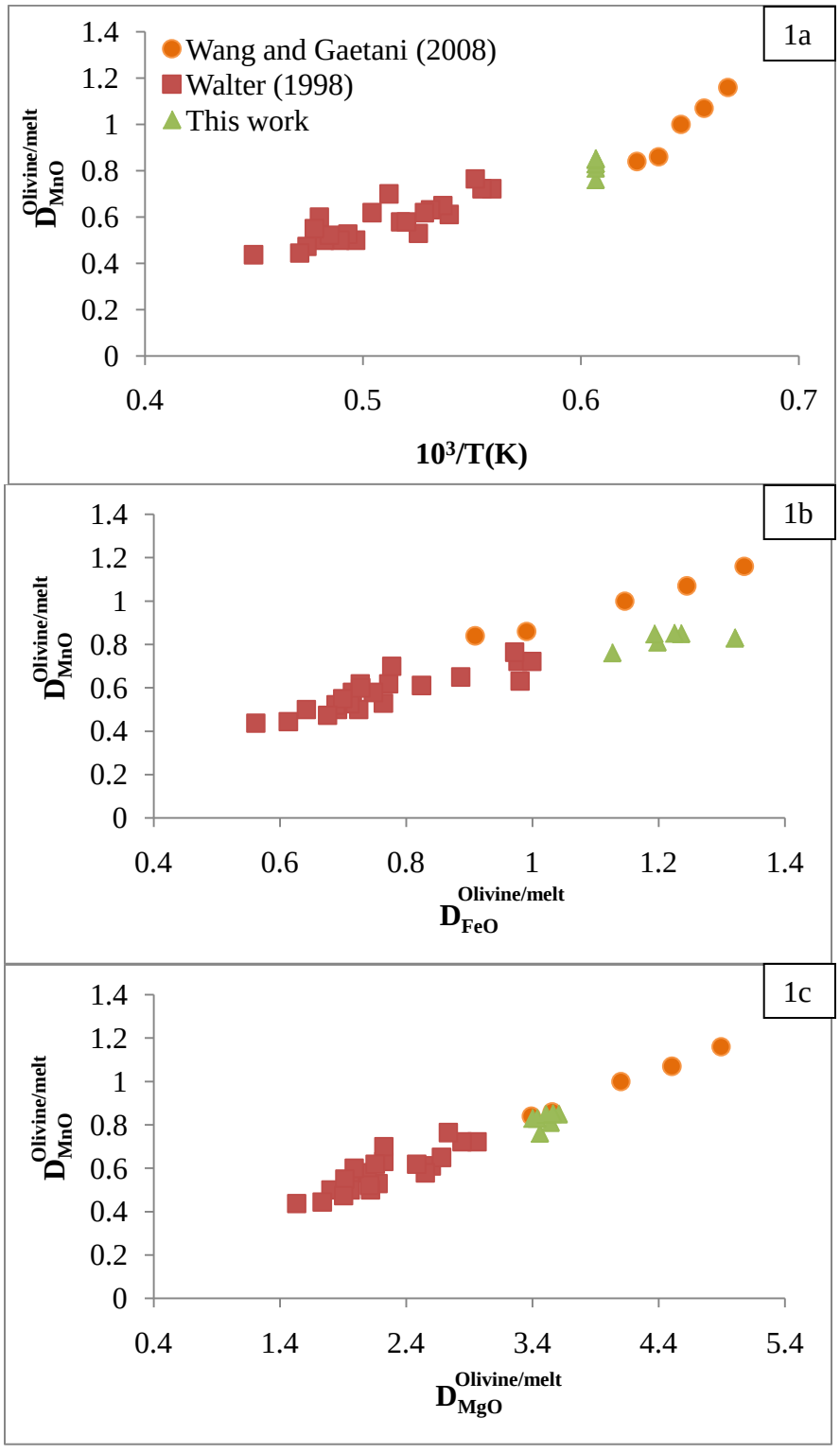


Figure 1

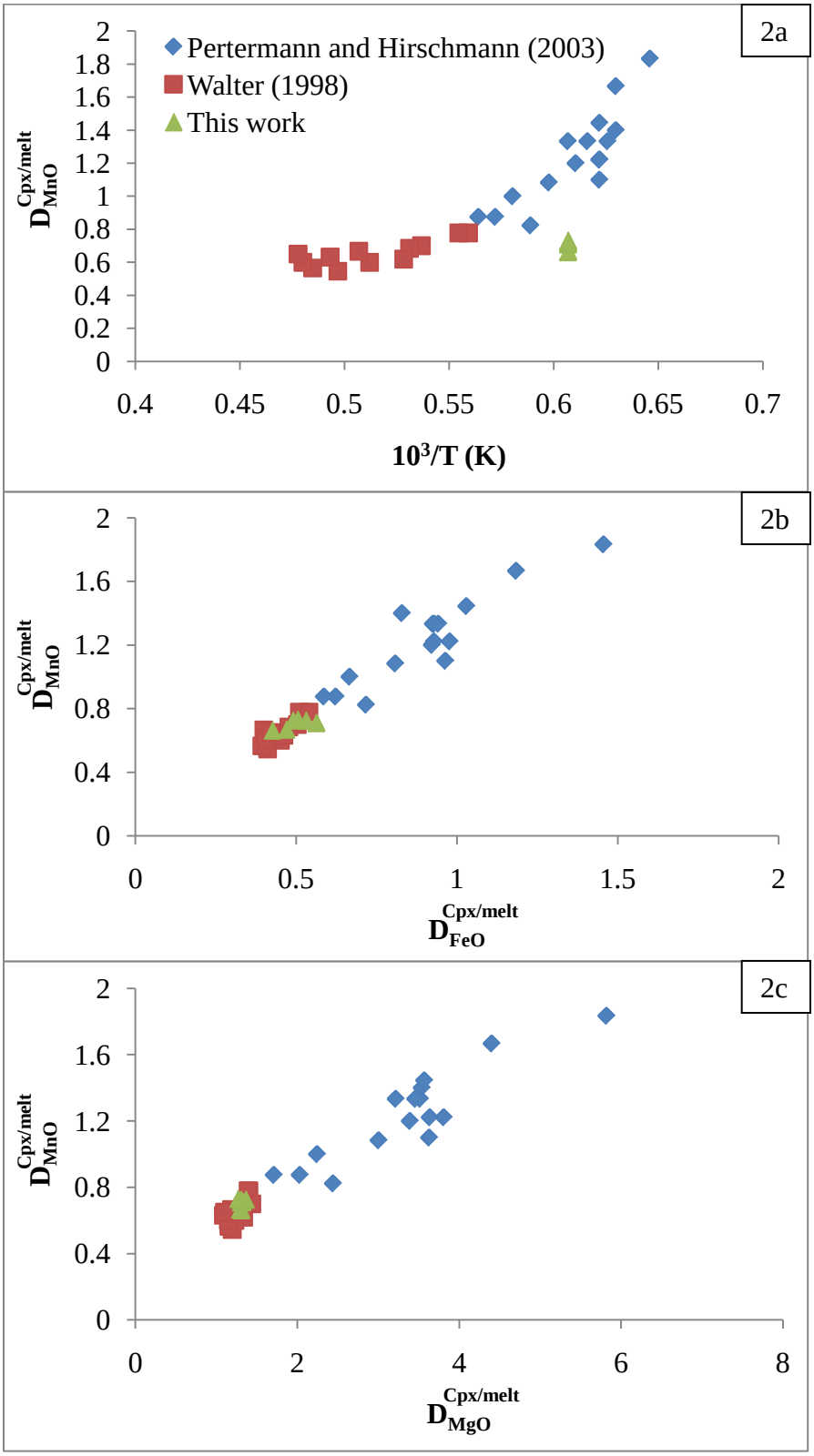
2a
Pertermann and Hirschmann (2003)
Walter (1998)
This work
$D^{Cpx/melt}_{MnO}$
$10^3/T$ (K)
2b
$D^{Cpx/melt}_{MnO}$
$D^{Cpx/melt}_{FeO}$
2c
$D^{Cpx/melt}_{MnO}$
$D^{Cpx/melt}_{MgO}$

Figure 2

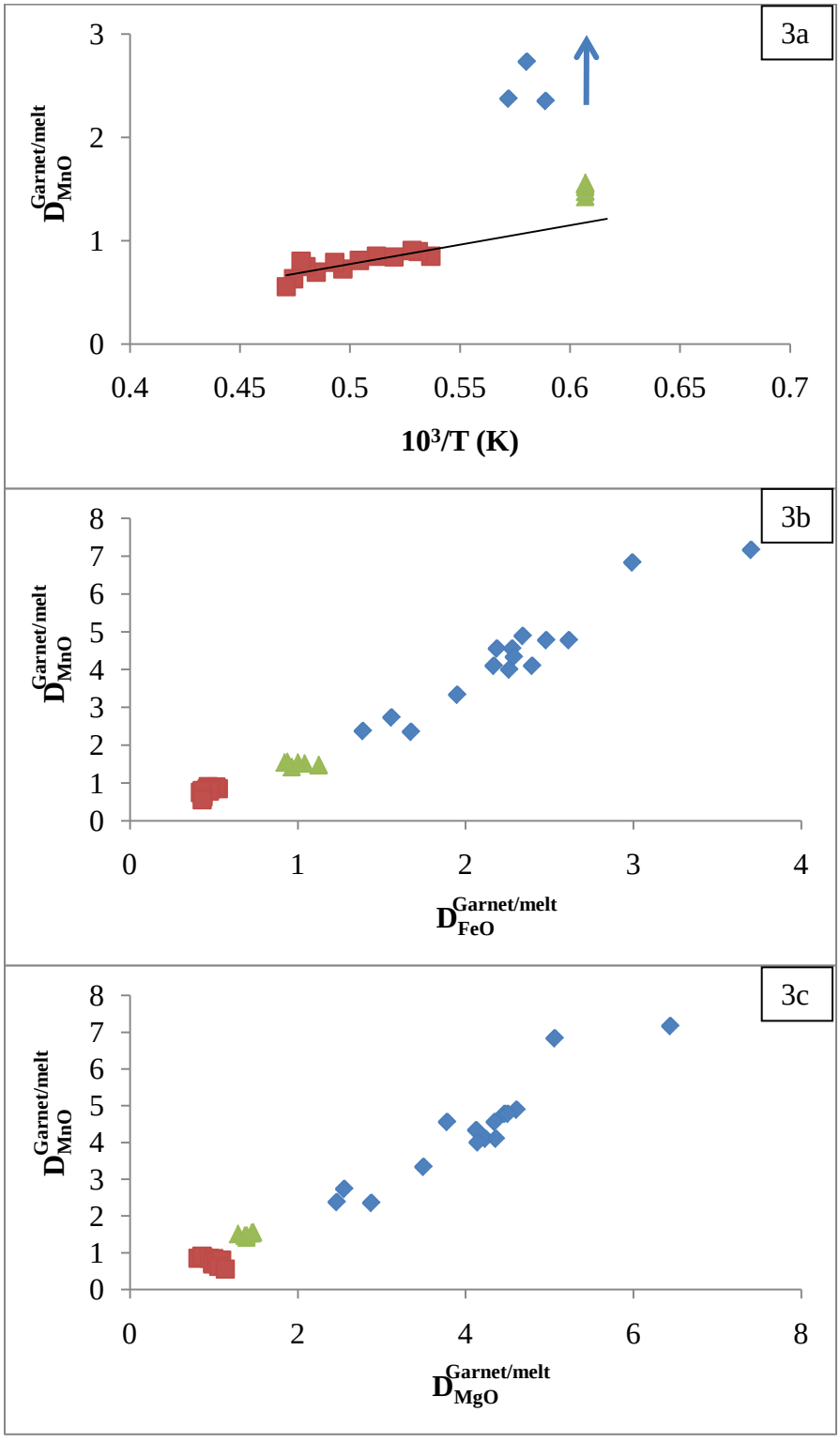
3a
$D^{Garnet/melt}_{MnO}$
$10^3$/T (K)
3b
$D^{Garnet/melt}_{MnO}$
$D^{Garnet/melt}_{FeO}$
3c
$D^{Garnet/melt}_{MnO}$
$D^{Garnet/melt}_{MgO}$

Figure 3

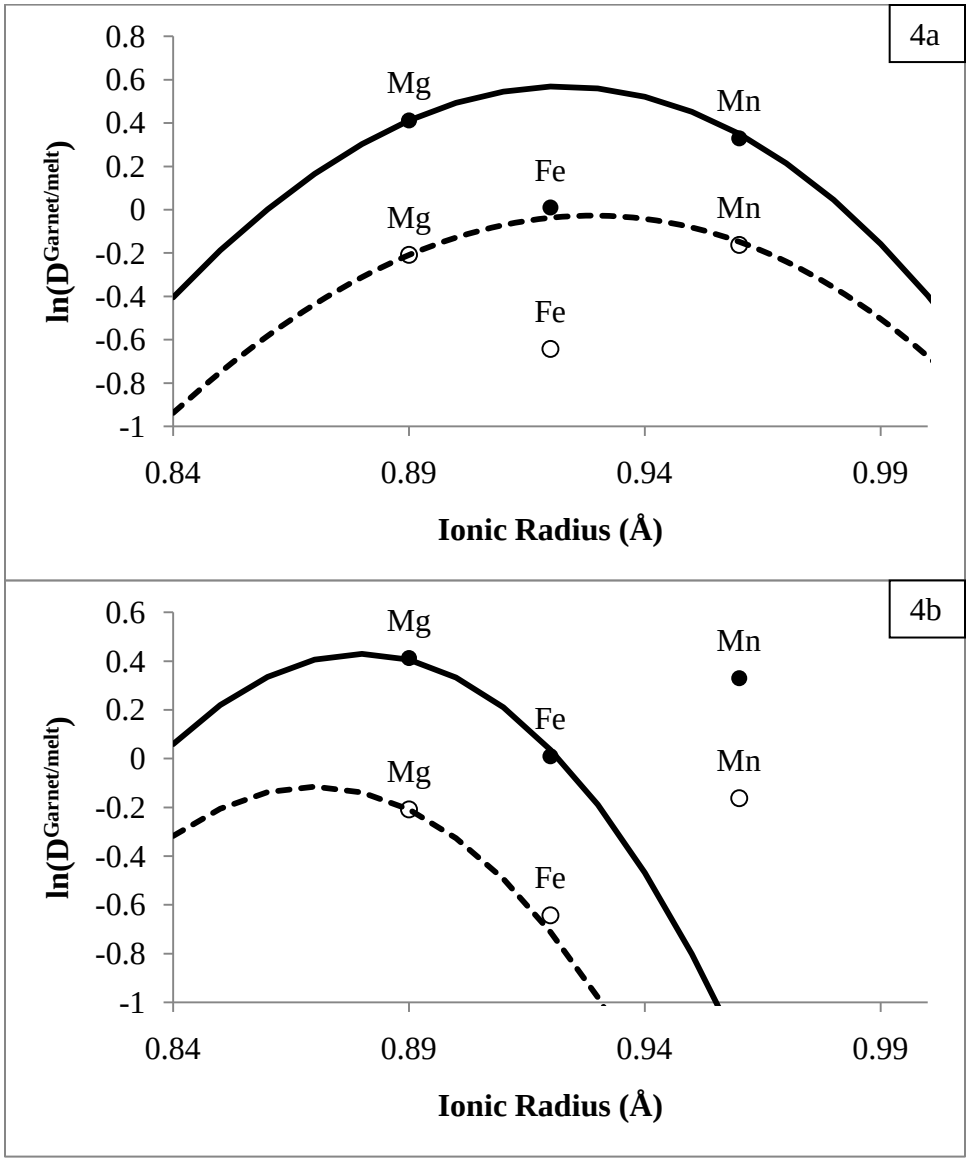
4a
0.8
0.6
0.4
0.2
0
-0.2
-0.4
-0.6
-0.8
-1
Mg
Mn
Fe
Mg
Mn
Fe
0.84
0.89
0.94
0.99
ln(D Garnet/melt)
Ionic Radius (Å)
4b
0.6
0.4
0.2
0
-0.2
-0.4
-0.6
-0.8
-1
Mg
Mn
Fe
Mg
Mn
Fe
0.84
0.89
0.94
0.99
ln(D Garnet/melt)
Ionic Radius (Å)

Figure 4

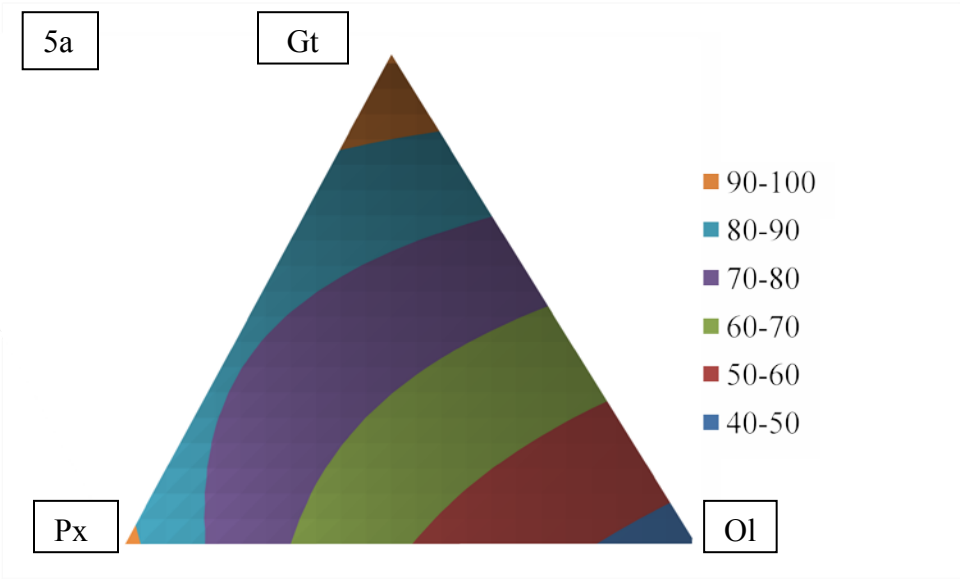
5a
Gt
90-100
80-90
70-80
60-70
50-60
40-50
Px
Ol

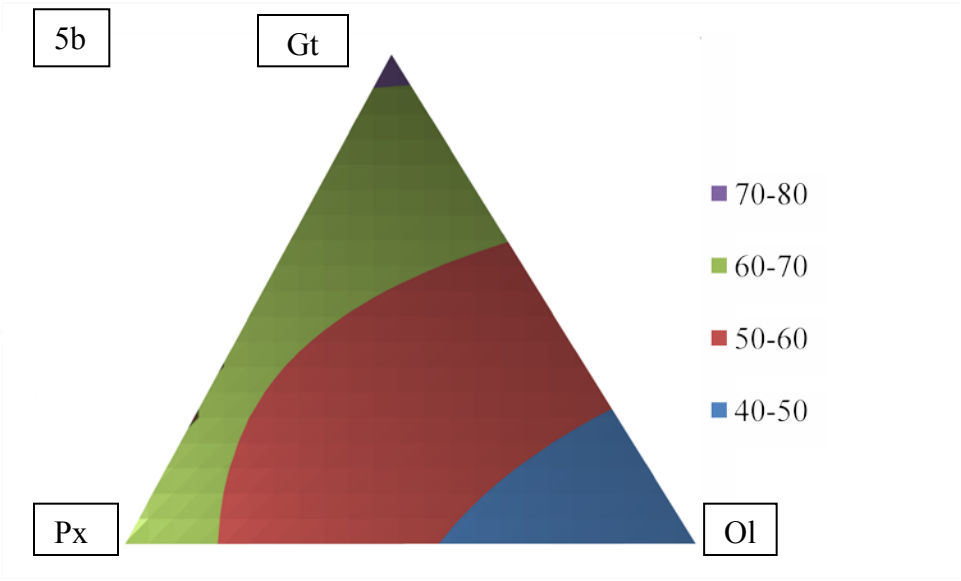
5b
Gt
70-80
60-70
50-60
40-50
Px
Ol

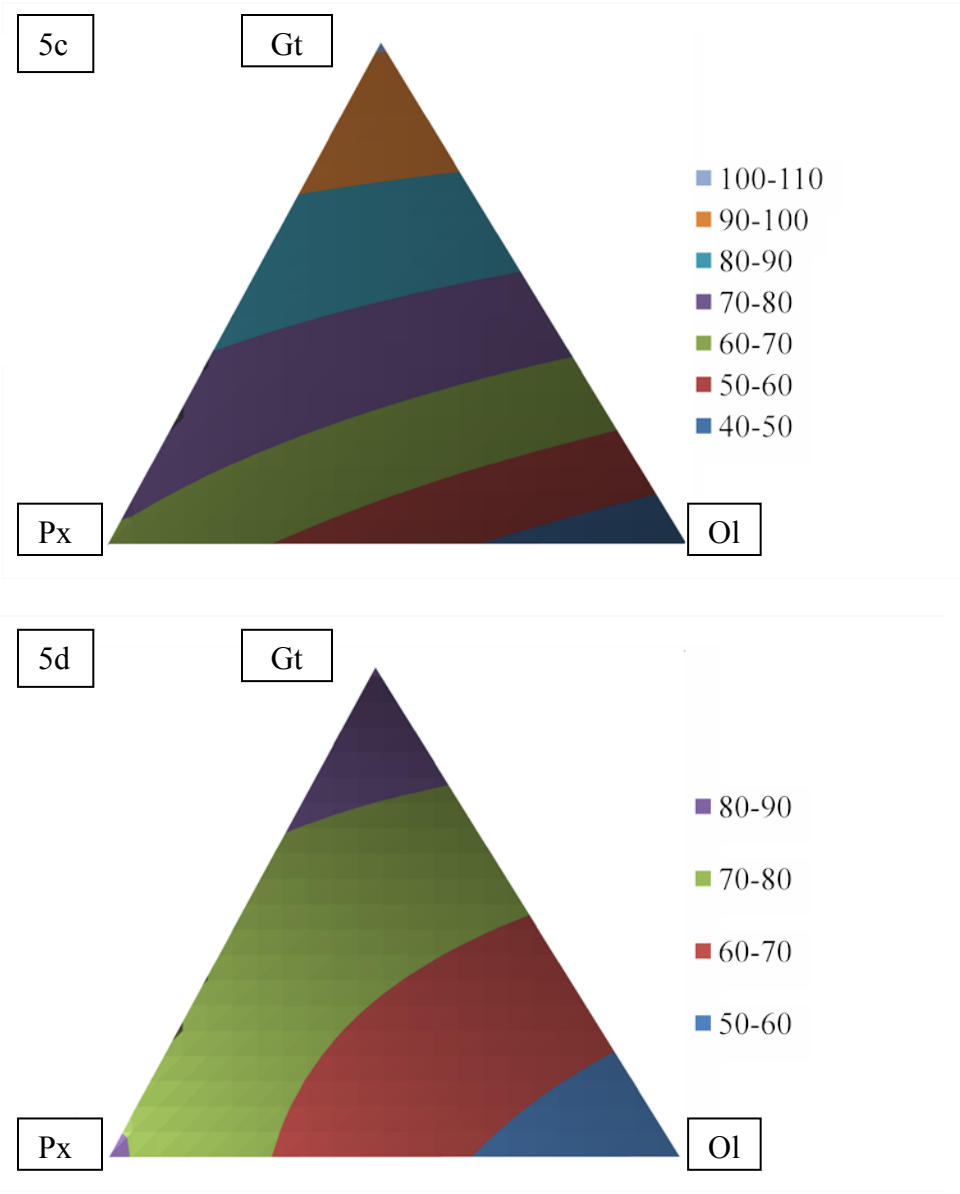
5c
Gt
100-110
90-100
80-90
70-80
60-70
50-60
40-50
Px
Ol
5d
Gt
80-90
70-80
60-70
50-60
Px
Ol

Figure 5

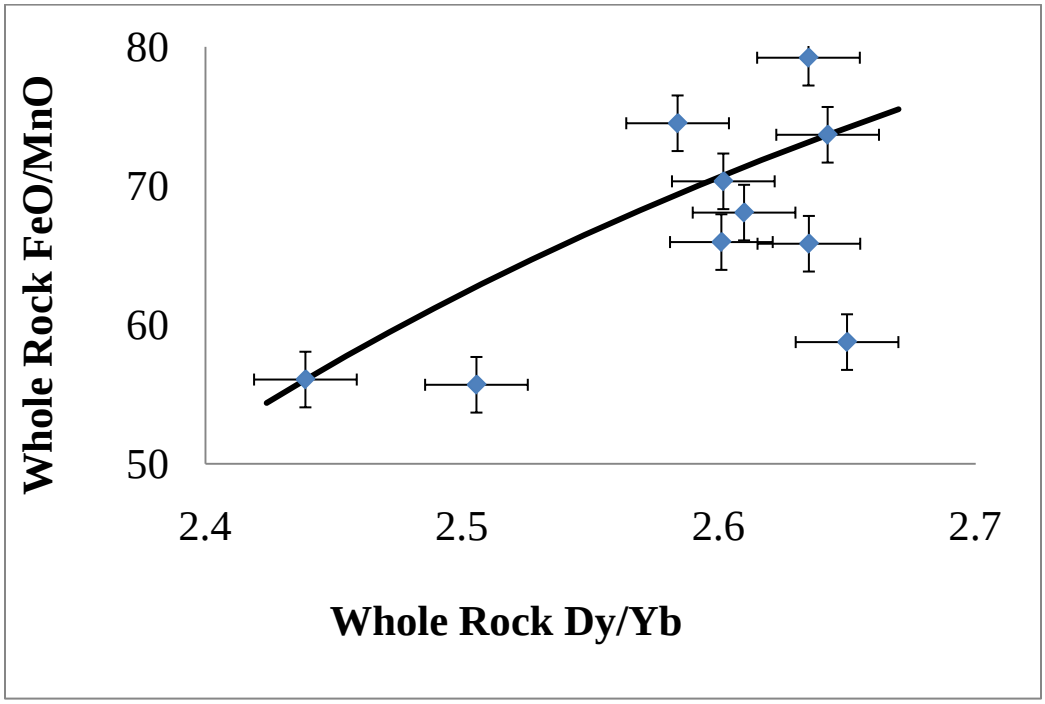


Figure 6